Structure of reduced and oxidized manganese superoxide dismutase: A combined computational and experimental approach

Rulisek, Lubomir; Ryde, Ulf

Published in:
The Journal of Physical Chemistry Part B

DOI:
10.1021/jp057295t

2006

Document Version:
Peer reviewed version (aka post-print)

Structure of reduced and oxidised manganese superoxide dismutase – a combined computational and experimental approach

Lubomír Rulíšek[a] and Ulf Ryde[b]

[a] Department of Molecular Modeling, Institute of Organic Chemistry and Biochemistry, Academy of Sciences of the Czech Republic, Flemingovo náměstí 2, 166 10 Praha 6, Czech Republic

[b] Department of Theoretical Chemistry, Lund University

Chemical Centre, P. O. Box 124 , S-221 00 Lund, Sweden

Correspondence to L. Rulíšek

E-mail: lubos@uochb.cas.cz

Tel: +420 – 220 183 263

Fax: +420 – 220 183 578

2017-04-10

Abstract

Manganese superoxide dismutases catalyses the disproportionation of the superoxide radical anion to molecular oxygen and hydrogen peroxide. Recently, atomic-resolution crystal structures of the reduced and oxidised enzymes have been reported. They show an active site with the manganese ion bound to one Asp, three His residues, and a solvent molecule. In this paper, we combine crystallographic refinement with quantum mechanical methods to show that the solvent ligand is undoubtedly a water molecule in the reduced state. However, the putative oxidised structure is to a large extent reduced during data collection, so that it contains a mixture of the Mn^{2+} and Mn^{3+} structure. The crystal structures show that the Mn-bound solvent molecule accepts a hydrogen bond from the side chain of the conserved Gln-146 residue. If the solvent ligand is water, this could lead to a steric clash, but the calculations indicate that such a clash is avoided by a tilt of the water molecule so that it forms an angle of 72° to the Mn–O bond. Such a conformation is also found outside the enzyme, giving a minimal destabilisation of the reduced state. We show by molecular dynamics simulations that the suggested Mn^{2+}–H_2O and Mn^{3+}–OH^- structures are stable. Moreover, we show that the superoxide substrate may bind both in the first coordination sphere of the Mn ion, opposite to the Asp ligand or in the second sphere, close to the conserved Tyr-34 and His-30 residues and ~5 Å from Mn. However, the second-sphere structures are not stable in long molecular dynamics simulations. We see no difference in the coordination between the reduced and oxidised states of the enzyme.

I. Introduction

The superoxide dismutases (SODs) catalyse the disproportionation of two molecules of the poisonous superoxide radical to molecular oxygen and hydrogen peroxide:

$$2\ O_2^{-\bullet} + 2\ H^+ \rightarrow O_2 + H_2O_2 \qquad (1)$$

They prevent oxidative damage by down-stream products of superoxide, such as the very reactive $OH^{\bullet}$ radical[1]. The SODs are found in all aerobic organisms. There are at least three unrelated families of SODs: the structurally homologous mononuclear iron and manganese SODs,[2,3] the binuclear copper–zinc SODs,[4] and the mononuclear nickel SOD.[5] The various SODs differ in terms of specific function. CuZnSODs are found in eukaryotic cytoplasm and are probably important for the clean-up of oxidative pollution from the immune system.[4,6] FeSODs are found in the periplasmic space of bacteria and in chloroplasts of plants, a few protists, and possibly in other eukaryotes, providing resistance to environmental or immunological oxidative stress.[2,7] MnSODs are found in bacteria and in the mitochondria of eukaryotes, where most of the O_2 is reduced. They are believed to protect DNA from endogenous oxidative stress.[3,8]

Several crystal structures of the manganese SODs (MnSODs) have been published.[3] They show that the enzyme is a dimer (prokaryotes) or tetramer (eukaryotes) of identical subunits. The active site consists of a Mn ion bound to one aspartate (Asp) and three histidine (His) residues. A solvent molecule, occupying the axial position opposite to one of the His ligands, completes the trigonal bipyramidal structure. The metal ion alternates between the Mn^{2+} and Mn^{3+} oxidation states: In one half-reaction, $O_2^{\bullet-}$ is oxidised to molecular oxygen and the metal ion is reduced to Mn^{2+}. In the other half-reaction, $O_2^{\bullet-}$ is reduced to H_2O_2 and the metal ion is oxidised to Mn^{3+}.[2]

Experimental studies have indicated that one proton is taken up by the enzyme in each half reaction.[3,9,10] It has been suggested that this proton is deposited on the metal-bound solvent molecule

during the first half-reaction, so that the solvent molecule is water in the reduced state of the enzyme, but a hydroxide ion in the oxidised state.[3,10,11,12] This suggestion has gained support from computational studies.[13,14,15] Thus, the two half-reactions of MnSOD can be described as:

$$Mn^{III}SOD–OH + O_2^- + H^+ \rightarrow Mn^{II}SOD–H_2O + O_2 \quad (2)$$

$$Mn^{II}SOD–H_2O + O_2^- + H^+ \rightarrow Mn^{III}SOD–OH + H_2O_2 \quad (3)$$

in which the metal-bound solvent molecule is explicitly shown. However, no direct evidence for this shift in the protonation state has yet been published.

In the present paper, we combine recent atomic-resolution (0.9 Å) crystal structures[16] with density-functional calculations to show that the reduced structure of MnSOD has a metal-bound water molecule. This is done by replacing the molecular mechanics force field, normally employed in protein structure refinement, with more accurate quantum mechanical calculations, quantum refinement.[17,18] By comparing the structures refined with both a water molecule and a hydroxide ion (i.e. refinements including hydrogen atoms in the active site), we show that the former structure fits the experimental and computational data best. This provides the first direct evidence for the protonation of the metal-bound solvent molecule in MnSOD. We have also studied the corresponding oxidised structure, but it turns out that this structure is partly reduced during data collection and therefore a mixture of Mn^{2+} and Mn^{3+}. Finally, we employ the structures to study the dynamics and hydrogen-bond pattern around the active site in the reduced and oxidised state, both without and with the superoxide substrate molecule.

II. Methods

Quantum refinement calculations

Quantum refinement[17,18] is essentially standard crystallographic refinement supplemented by quantum mechanical (QM) calculations for a small part of the protein. Crystallographic refinement programs change the protein model (coordinates, occupancies, *B* factors, etc.) to improve the fit of

the observed and calculated structure-factor amplitudes (usually estimated as the residual disagreement, the *R* factor). Owing to the limited resolution normally obtained for biomolecules, the experimental data are supplemented by chemical information, usually in the form of a molecular mechanics (MM) force field.[19] Thus, the refinement takes the form of a minimisation or simulated annealing calculation using an energy function of the form

$$E_{cryst} = w_A E_{Xref} + E_{MM} \quad (4)$$

where E_{Xref} is a penalty function, describing how well the model agrees with the experimental data (we used the maximum-likelihood refinement target using amplitudes, *MLF*[20,21]), E_{MM} is a MM energy function with bond, angles, dihedral, and non-bonded terms, and w_A is a weight factor, which is necessary because E_{MM} is in energy units, whereas E_{Xref} is in arbitrary units.[22]

Quantum chemistry can be introduced in this function by replacing the MM potential for a small (but interesting) part of the protein (system 1) by QM calculations, yielding a QM energy for system 1, E_{QM1}. To avoid double counting, we must then subtract the MM energy of system 1, E_{MM1}:

$$E_{tot} = E_{QM1} - E_{MM1} + E_{MM} + w_A E_{Xref} \quad (5)$$

Thereby, we introduce an accurate energy function for the system of interest. Such an energy function is implemented in the program ComQum-X,[17] which is a combination of the software Turbomole[23] and Crystallography and NMR system (CNS).[24] Following crystallographic custom, hydrogen atoms and electrostatic interactions were ignored in the refinements, but hydrogen atoms are present in the QM calculations of system1.

ComQum-X has been tested by re-refining the structure of *N*-methylmesoporphyrin bound to ferrochelatase.[17] The results showed that we may improve the structure locally in terms of the R_{free} factor. Moreover, we have shown[25] that refinement with ComQum-X of a medium-resolution (1.7 Å) crystal structure of cytochrome c_{553} brings the geometry of the haem group and its ligands closer to that observed in an atomic-resolution structure (0.97 Å) of the same protein. For example, the errors in the Fe–ligand distances are reduced from 0.03–0.09, 0.12, and 0.32 Å to 0.01, 0, and 0.02

Å (for the porphyrin, histidine, and methionine ligands, respectively). We have also shown that we can decide the correct protonation status of metal-bound solvent molecules with this method, both for a zinc-bound water and an alkoxide in alcohol dehydrogenase.[26] The COMQUM-X program is available from the authors by request (but the Turbomole and CNS software have to be obtained separately).

The protein

All calculations reported in this paper are based on the atomic-resolution (0.9 Å) crystal structures of the Tyr174Phe mutant of MnSOD from Escherichia coli in the reduced and oxidised state (protein data bank accession codes 1ix9 and 1ixb).[16] The mutation is ~9 Å from the Mn ions, at the dimer interface and the mutant has ~40% of the wild-type activity.[27] Coordinates, occupancies, and *B* factors were downloaded from the protein data bank, whereas the corresponding structure factors were generously provided by Prof. G. B. Jameson. From these files, we obtained the space group, unit-cell parameters, resolution limits, *R* factors, and the selection of reflections for the calculation of the R_{free} factor. All quantum-refinement calculations included the alternate conformations in the original files.

The full geometry of the proteins (dimers of a total of 410 amino acid and 925 water molecules) was optimised, using the same convergence criteria as in the vacuum QM calculations. In each cycle of the geometry optimisation, the surrounding protein was allowed to relax by one cycle of crystallographic minimisation and one cycle of individual *B*-factor refinement. However, the new coordinates and *B* factors were accepted only if the *R* factor was reduced. For the protein, we used the standard CNS force field (protein_rep.param, water.param, and ion.param). For the other program parameters, we used data from the PDB files or the default choices. Residue (real-space) *R* factors[28] were calculated with CNS from σ_A-weighted maps, in which the Mn ion and its ligands were omitted. For the w_A factor, we used the default choice of CNS, 0.0432 for the reduced structure

and 0.0475 for the oxidised structure.

Quantum chemical calculations

All quantum chemical calculations were performed with the density functional Becke-1988 – Perdew-1986 method (BP86),[29,30] as implemented in the Turbomole package. These calculations employed the 6-31G* basis set for all atoms,[31] except for Mn, for which we used the DZP basis sets of Schäfer et al.[32] The structures were optimised until the change in energy between two iterations was below 2.6 J/mole (10^{-6} a.u.) and the maximum norm of the internal gradients was below 5.0 kJ/mole/Å (10^{-3} a.u). All complexes were studied in the high-spin state, employing unrestricted open-shell theory.

Density functional methods have been shown to give excellent geometries for transition metal complexes, with errors in the bond distances of 0–0.07 Å.[25,33,34,35,36] Calibrations on similar metal complexes have shown that the geometries and energies do not change significantly if the method or the basis sets are improved from the present level.[37]

The His ligands were modelled by imidazole (Im), whereas the Asp ligand was modelled by an acetate ion (Ac). In addition, the Gln-146 residue, which forms a hydrogen bond to the solvent molecule was also included in the calculations as a acetamide (Am) molecule. The quantum system is shown in Figure 1.

The same QM system was used in the quantum refinement calculations. This means that there are five bonds between the QM and MM systems. These were treated by the hydrogen link-atom approach,[38,39] in which the QM system is truncated by hydrogen atoms, the positions of which are linearly related to the corresponding carbon atoms in the full system.

Molecular dynamics simulations

Molecular dynamics (MD) simulations were run on the best quantum refined structures using

the Amber 8 software[40] and the Amber ff03 force field.[41] In these calculations, all alternate conformations were deleted, keeping the one with the highest occupancy. Hydrogen atoms were added by Amber, assuming that all Asp and Glu residues are negatively charged and all Lys and Arg residues are positively charged. The protonation status of the His residues were determined by a study of the hydrogen-bond pattern, the surroundings, and the solvent exposure of each residue: His-17, 26, 30, 81, and 171 was assumed to be protonated on the $N^{\delta 1}$ atom, whereas the other residues (His-27, 31, and 78) were assumed to be protonated on the $N^{\varepsilon 2}$ atom (the crystal structures were determined at pH 8.5). This choice made the whole protein neutral in the Mn^{2+}–H_2O and Mn^{3+}–OH^- complexes.

The proteins were solvated in a sphere of explicit TIP3P water molecules with a radius of 45 Å (6 Å outside any residue in the protein). About 8430 water molecules were added to the two proteins, giving ~34380 atoms in the simulations. The added water molecules were kept inside the sphere by a force constant of 6.3 kJ/mole/Å^2 (42 kJ/mole/Å^3 with the reaction field). The structures were first minimised and then equilibrated for 20 ps, restraining heavy atoms of the proteins to the crystal structure by a force constant of 209 kJ/mole/Å^2. Then, the restraint was removed and the structures were equilibrated for 200 ps and coordinates were collected each 10 ps during ~1000 ps.

In all MD simulations, bonds involving hydrogen atoms were kept fixed at their equilibrium values[41] by the SHAKE algorithm. The time step in the MD simulations was 2 fs. The temperature was kept constant at 300 K using a weak coupling to a temperature bath using a time constant of 1 ps.[42] A cut-off for the non-bonded interactions of 15 Å was employed and non-bounded pair list was updated every 50 ps. The 1-4 electrostatic and van der Waals interactions were scaled by a factor of 1.2 and 2.0, respectively. A dielectric constant of 1.0 was used in all simulations.

Charges for the Mn ion and its ligands (separate for the oxidised and reduced states) were taken from QM calculations without the Glu-146 model. The QM electrostatic potential was calculated in 10 000 random points up to 8 Å from the molecule. The charges were then fitted to these potentials, using a Boltzmann weight for points close to the active-site model. In the fit, it was ensured that the

total charge and dipole moment was exactly reproduced, whereas the fit was restrained to reproduce also the quadrupole and octupole moment (the CHELP-BOW procedure).[43] The resulting charges are collected in Table S1 in the supplementary material. The $O_2^{-\bullet}$ molecule was modelled as an isolated ion (i.e. with the same charge on the two oxygen atoms, 0.5 *e*).

After some test calculations, we decided that the most reliable results for the active site in the MD simulations were obtained if explicit bonds were defined between the Mn ion and its first-sphere ligands and if non-zero force constants were used for the bonds and angles, whereas no dihedral restraints were introduced. Similar models have been used for other metal sites.[44] The equilibrium parameters and force constants used for the reduced and oxidised sites are collected in Table S2. The equilibrium parameters were taken from the crystal structure (reduced state) or from QM optimised structures (oxidised site). Force constants were extracted from the Hessian matrix taken from a QM frequency calculation of the optimised structures, using the method of Seminario[45] (program Hess2FF[44]). Different parameters were used for the three His ligands.

III. Results and Discussion

Quantum refinement of the reduced structure

We started by performing a re-refinement of the two atomic-resolution structures of MnSOD in the putative reduced and oxidised states of the enzyme. The aim of this investigation was to decide the protonation state of the metal-bound solvent molecule. Therefore, we re-refined the structures with both a metal-bound water molecule and a hydroxide ion in the QM system, and then we tried to decide which of the two structures fit the experimental data best by studying the *R* factors, the strain energy, and the difference in metal–ligand distances between the structures optimised in the protein and in vacuum.[26] The results are collected in Table 1.

For the reduced protein, the results are quite conclusive: The structure with a Mn-bound water molecule fits the experimental data better than that with the Mn-bound OH^- ion according to all six

quality criteria. First, the former structure gives a lower value for both the R_{free} factor (0.2155 compared to 0.2157) and the standard R factor (0.2078, compared to 0.2079). The difference is not large, because the R factors are global factors that are quite insensitive to small local changes. However, our previous experience has shown that these small variations in the R and R_{free} factors are in accordance with the other quality criteria and therefore actually seem to be significant.[17,18,25,26] It is also notable that the re-refinements slightly improve the R_{free} factor, compared to the original crystal structure (0.2155, compared to 0.2158), but the R factor increases somewhat (from 0.2077 to 0.2078). This is also normally observed and in both cases indicate a slight improvement of the structure, owing to the replacement of the MM force field with the more accurate QM calculations (the decrease in the difference between R and R_{free} indicates that overfitting has been reduced).[17,18,25,26]

Much larger differences are seen in the more local real-space (residue) R factor,[28] calculated from an omit map of the protein without the metal and its ligands: The real-space R factor of the solvent molecule is 0.051 for the water structure, but 0.056 for the OH^- structure. The real-space R factor for the other residues were essentially identical for the two structures.

Third, the water structure gives an appreciably smaller ΔE_{QM1} energy, 34 compared to 94 kJ/mole. ΔE_{QM1} is the difference in QM energy of the QM system, optimised in vacuum and in the protein and therefore indicates how well the optimum structure fits into the protein. It was calculated after the removal of the Gln-146 ligand mode, because this second-sphere ligand may move quite extensively in the vacuum optimisations (but results including this ligand showed the same trends).

Fourth, we looked at the metal–ligand distances and compared them with those obtained in a vacuum optimisation. From Table 2, where the distances are listed, it can be seen that all five distances in the water structure are within 0.07 Å of those obtained in vacuum (absolute sum of the deviations is 0.19 Å). The largest differences are observed for the second His ligand (0.07 Å) and for the water molecule (0.05 Å). These are quite typical differences: our previous investigations

have indicated that QM calculations in vacuum reproduce metal–ligand bond lengths within 0.07 Å for similar Fe, Ni, and Cu systems.[25,33,34,35,36] However, the OH^- structure gives much larger differences of 0.12–0.17 Å, except for the Asp ligand (0.03 Å), with a absolute sum of the deviations (0.62 Å) that is over three times larger than for the water structure.

Likewise, the metal–ligand bond lengths in water structure are most similar to those in the original crystal structure: The largest difference is only 0.02 Å and the absolute sum of all five distances is only 0.05 Å (showing that the original crystal structure is accurate and the QM restrains have little effect, owing to the high resolution). For the corresponding OH^- structure, the Mn–O_{Sol} distance differs by 0.12 Å from the original crystal structure, showing that the ideal distance for a Mn^{II}–OH^- bond is (1.98 Å) is incompatible with the crystallographic data.

Finally, we also looked at the electron density maps of the two re-refined structures. As can be seen in Figure 2, the $f_o - f_c$ difference maps show much larger deviations for the OH^- structure (green and yellow volumes) than for the water structure (blue and red volumes). Thus, we can safely conclude that the reduced crystal structure contains a metal-bound water molecule.

Quantum refinement of the oxidised structure

Next, we looked at the oxidised crystal structure. Quite unexpectedly, the results for this structure were much harder to interpret than for the reduced structure. For example, the R_{free} factors of both the water and OH^- structure increased, compared to the original structure (0.2128–0.2130, compared to 0.2125), indicating that the structure is not improved by QM. Likewise, both structures showed quite large deviation in the metal–ligand distances from those obtained in vacuum (e.g. 0.09 and 0.11 Å for the Mn–O_{Sol} distances). This indicates a significant misfit between the crystal structure and the QM calculations.

In all water structures, there is a hydrogen bond between the water ligand and the non-ligating atom of the Asp ligand. This is also observed in the crystal structures.[3] Interestingly, it turns out that

in the Mn^{3+}–H_2O structure, the proton involved in this hydrogen bond actually moves to the Asp ligand, giving a protonated (neutral) acetate and a OH^- ion (indicated by AspH–OH^- in the tables). It is conceivable that this is a pure vacuum effect and that the misfit between the QM structures and the crystallographic data is caused by the fact that we actually do not model a true Mn^{3+}–H_2O state. Therefore, we also re-refined a structure with the Mn^{3+}–H_2O state, induced by a restraint in the O–H bond. However, it can be seen from Table 1 (H_2O state) that this led only to minor improvements in the *R* factors, and strongly increased ΔE_{QM1} energy.

Another explanation for the misfit is that the crystal structure has been partly reduced during data collection. During the crystallographic data collection, a significant amount of the X-ray photons deposit their energy into the crystal lattice, giving rise to secondary electrons which may change the redox-state of metalloproteins.[46] In fact, it has been suggested before that oxidised structures of MnSOD are partly reduced.[14,47,48] Therefore, we also re-refined the oxidised structure with Mn^{2+} and either water or OH^- in the QM system.

These reduced structures gave somewhat better results. For example, R_{free} was reduced to 0.2122 in the $Mn^{II}H_2O$ structure, and the difference in the Mn–O_{Sol} distance between crystal and vacuum was reduced to 0.04 Å. This structure also had the lowest deviation form the original crystal structure, but both the maximum deviation (0.06 Å) and the absolute sum of the deviations (0.11 Å) were 2–3 times larger than for the reduced crystal structure. Moreover, the other criteria pointed out different structures as the best ones: the $Mn^{II}OH^-$ structure had the lowest value for the *R* and real-space *R* factors, whereas the $Mn^{III}OH^-$ structure had the lowest sum of absolute deviations in the metal–ligand distances. This quite strongly indicates that the crystal structure is a mixture of oxidation and protonation states, as can be expected if the structure is successively reduced during data collection. Most likely, it is a mixture of the $Mn^{III}OH^-$ and the (dominant) $Mn^{II}H_2O$ structure. This would explain why both water and OH^- structures give the best results for the various quality criteria.

Thus, we can conclude that ComQum-X is sensitive to disorders in the QM system. On the

other hand, it is a powerful method to detect such disorders, which is highly important for the interpretation of the structure: If the active site is disordered, it means that the crystal structure is unreliable, in the meaning that the details of the structure cannot be trusted, because it is a mixture of several atomic states. This is nicely illustrated by the present structure, which shows a $Mn–O_{Sol}$ distance of 2.12 Å, i.e. in between the QM vacuum distances for $Mn^{III}–OH^-$ (1.78 Å) and $Mn^{II}H_2O$ (2.23–2.27 Å).

Hydrogen-bond network around the active site

The ligands of the active Mn site in MnSOD are stabilised by several hydrogen bonds to the surrounding protein (Figure 3). Two of the His ligands form hydrogen bonds with their non-ligating $N^{\delta 1}$ atom to residues in the surrounding protein (His-81 to O in Gly 77 at 2.7 Å and His-171 to OE2 of Glu-170 from the other subunit at 2.7 Å, thereby compensating the +1 charge of the metal site), whereas the last His residue (His-26) forms a hydrogen bond to a water molecule instead (2.7 Å).

The Asp-167 ligand forms a hydrogen bond to the solvent ligand (2.7–2.8 Å) and a weaker interaction with the backbone of Trp-169 (3.1 Å). The solvent ligand itself forms hydrogen bonds with $N^{\varepsilon 2}$ of Gln-146 (2.9–3.0 Å). Asp-167 is a hydrogen-bond acceptor and Gln-146 is a donor, giving a perfect hydrogen-bond network for a Mn-bound OH^- ion (Figure 4a).

However, for a Mn-bound water molecule, an additional acceptor is missing: There are no further acceptors in the crystal structure within 4 Å of the solvent molecule (the closest water molecule is 5.3 Å away). Furthermore, it is unlikely that Gln-146 will rotate to expose its acceptor $O^{\varepsilon 1}$ group towards the solvent molecule, because it forms hydrogen bonds to $N^{\varepsilon 1}$ of Trp-128 (2.9 Å) and to $N^{\delta 2}$ of Asn-80 (3.2 Å), both hydrogen donors (Figure 3). The $N^{\varepsilon 2}$ atom of Gln-146 also forms a hydrogen bond to the side-chain OH of Tyr-34 (2.9 Å), which in its turn forms a hydrogen bond to water molecules (2.5–2.7 Å), at the bottom of a solvent-filled entrance channel to the active site. Thus, the crystal data indicates that the hydrogen-bond network is designed to satisfy a metal-bound

OH^- ion, but not a water molecule.

This is potentially a serious problem, because there would be a severe steric clash between the two hydrogen atoms on the water ligand and on the $N^{\varepsilon 2}$ atom of Gln-146 (0.9 Å if the two hydrogen atoms both are along the O_{sol}–$N^{\varepsilon 2}$ bond. This was the reason why we included the Gln-146 model in our quantum refinements (remember that hydrogen atoms are explicitly considered in the quantum system). As can be seen in Figure 4b, the problem is solved by tilting the HOH plane 72° away from the Mn–O_{Sol} bond. Thereby, the water ligand can still form the hydrogen bonds to Asp-167 and Gln-146 (1.54 and 2.00 Å H–O distances; they are 1.81 and 2.06 Å in the corresponding Mn^{3+}–OH^- structure), but also avoiding a steric clash (the H–H distances is 2.26 Å; this is longer than what was obtained previously by only partial optimisations, 1.89 Å.[49] In fact, this is close to the optimum vacuum structure of this complex: If the Gln-146 model is removed and the hydrogen atom of the water ligand, not directed towards Asp-167 is reoptimised, less than 1 kJ/mole is gained. Likewise, in the fully optimised structure of that complex, the angle between the HOH plane and the Mn–O_{Sol} bond is only 4° smaller. Thus, we can conclude that the active-site Mn ion in MnSOD easily can bind also a water molecule, without any appreciable strain in the structure. The only destabilising factor in such a complex is that one of the hydrogen atoms in the water ligand is not involved in any hydrogen bonds.

In order to further test if this is a correct interpretation and if the hydrogen-bond structure suggested by the crystal structure is reasonable, we have run molecular dynamics simulations of the MnSOD enzyme, both in the Mn^{III}–OH^- and Mn^{II}–H_2O states. The results of these simulations are described in Table 3. They show that both the hydrogen bonds involving the OH^- ligand (to Asp-167 and to Gln-146) are stable during the simulations of the oxidised enzyme: The former bond is ~2.05 Å on average, whereas the other bond is 2.08 Å. Both hydrogen bonds are present during the whole simulation, but the fluctuations are somewhat larger for the bond to Asp-167.

For the reduced structure with H_2O, the results are similar for the hydrogen bond from Gln-146.

However, for the hydrogen bond to Asp-167, the results show that both hydrogen atoms in the water ligand are involved in this interaction, although not at the same time. Approximately, every 50 ps the hydrogen bonding atom is switched. This probably reflects the fact that there is no alternative hydrogen-bond partner for the hydrogen atom for the other hydrogen atom of the water ligand. However, most importantly, the results show that the structures obtained in the quantum refinements are stable during a 1 ns MD simulations and therefore are reasonable.

Substrate binding

Finally, we have also performed some preliminary simulations of the binding of the $O_2^{-\bullet}$ substrate to both oxidised and reduced MnSOD. A conceivable interpretation of the missing hydrogen bond for the water structures is that it is intended to stabilise the binding of the substrate, perhaps stabilising different coordination modes in the reduced and oxidised states of the enzyme. The MnSOD reaction is so rapid that it has been impossible to study reaction intermediates with spectroscopic method. Therefore, the binding of a number of small molecules with some similarity to the $O_2^{-\bullet}$ substrate have been studied instead, in particular N_3^-, $NO^\bullet$, and F^-.[47,50,51,52] Unfortunately, they have given partly conflicting results, pointing to both first- and second-sphere binding, depending on the ligand, the oxidation state, and the enzyme (Mn or FeSOD). In addition, recent QM calculations have indicated a small intrinsic preference for a second-sphere pathway for the second half-reaction of the enzyme (starting from Mn^{2+}).[53]

Therefore, we have performed a series of MD simulations of MnSOD in the reduced and oxidised states, including the $O_2^{-\bullet}$ substrate. The simulations were started with the substrate in three different positions. In the first, $O_2^{-\bullet}$ was bound to the Mn ion at a Mn–O distance of ~2.2 Å, in the open coordination site opposite to the Asp-167 ligand (where N_3^- or an extra solvent molecule binds.[50,54,55] In the second, $O_2^{-\bullet}$ was put in the second-coordination sphere between Tyr-34 and His-30, where a prebinding site has been suggested.[2,56] In the third, $O_2^{-\bullet}$ was put at a hydrogen-bond

distance from the solvent molecule, directed towards Tyr-34. All these structures (with one $O_2^{-\bullet}$ ion in each of the two subunits of the enzyme) were equilibrated for 200 ps and then simulated for 1 ns. In total, 12 structures will be discussed, viz. those of the metal ions in each of the two monomers in the simulation of the three binding modes and the two oxidation states.

Three different coordination modes were observed in these simulations, as are illustrated in Figure 5. In the first (obtained in eight of the simulations, viz. all with the two first starting structures in both oxidations states), the $O_2^{-\bullet}$ molecule binds directly to the Mn ion in a side-on mode. The Mn–O distances are both ~2.2 Å. However, this should not be taken as an evidence that the side-on binding mode of $O_2^{-\bullet}$ is more favourable than the end-on mode in the protein. The relative preference of the two binding modes can only be determined by QM methods, in which electron-flow between the two oxygen atoms is allowed and the ligand-field and the electronic structure of the metal ion are considered. In the present MD simulations, such effects are not included and the two oxygen atoms in $O_2^{-\bullet}$ have the same charge, thereby making the side-on binding more favourable. In QM optimisations of the $MnIm_3Ac(H_2O/OH)O_2$ state in vacuum, $O_2^{-\bullet}$ prefers to bind in a end-on mode with Mn–O distances of 1.92 and 2.80 Å (oxidised) or 2.19 and 2.97 Å (reduced).[53] However, the MD simulations show that there actually is room of a side-on binding of $O_2^{-\bullet}$ in the enzyme and therefore also for the less sterically demanding end-on mode. In the simulated structures, the $O_2^{-\bullet}$ molecule forms hydrogen bonds to Tyr-34 (2.0–2.2 Å), some water molecules close to Tyr-34 (~2.0 Å), and sometimes to the Mn-bound water molecule (1.8–1.9 Å) or His-30 (~1.9 Å).

In the second group of binding modes (two simulations, viz. those of the third starting structure in subunit A, for both the oxidised and reduced states), $O_2^{-\bullet}$ has left the active site and becomes fully solvated.

In the third binding mode (two simulations), $O_2^{-\bullet}$ binds in the second coordination sphere of Mn, with Mn–O distances of 5.2 and 6.1 Å (Figure 5b). This binding mode is stabilised by a

hydrogen bond to Tyr-34 (1.7 Å) and to several water molecules in the active site (1.7–1.9 Å). In the reduced structure, this binding mode is also stabilised by a hydrogen bond from $H^{\delta 1}$ atom of His-30 (2.0 Å). This residue has different conformation in the two subunits of this high-resolution MnSOD structure (it is turned 180°). Only in the second subunit does the $N^{\delta 1}$ atom point upwards towards Tyr-34, and only in this subunit is this binding mode of $O_2^{-\bullet}$ encountered. However, in the oxidised structure, this binding mode is also observed only for the second subunit, but in this structure, His-30 has the same configuration in both subunits and there is no hydrogen bond between His-30 and $O_2^{-\bullet}$. In this binding mode of $O_2^{-\bullet}$, no interaction between the Mn-bound water molecule and $O_2^{-\bullet}$ is observed (O–O distance of ~4.4 Å). This binding mode can probably be more trusted, because it does not involve any binding to Mn. However, both in the reduced and oxidised proteins, this coordination mode turned out to be unstable and reorganised after 300–600 ps to one of the other two binding modes, first-sphere binding for the reduced protein and dissociation for the oxidised protein.

Thus, we can conclude that it is possible to obtain both a first- and a second-sphere binding of $O_2^{-\bullet}$ to MnSOD, but first-sphere binding seems to be much more stable. However, the present data is too incomplete to rule out the possibility of second-sphere binding of the substrate. In our simulations, we do not see any clear difference between the oxidised and reduced structures (the two binding modes are obtained in exactly the same simulations for the two oxidation states).

IV. Conclusions

We have performed a detailed study of the recent atomic-resolution crystal structures of MnSOD.[16] First, we combined the crystallographic raw data with quantum chemical calculations (quantum refinement[17,18]) to show that in the reduced structure, the solvent ligand undoubtedly is a water molecule. This has widely been assumed before[3,12,57] and it has been supported by indirect experimental data (e.g. that a proton is taken up by the enzyme upon reduction, but not by Tyr-34,

which is the most plausible alternative to the solvent ligand),[9,11,11] as well as by QM estimates of the pK_a value of the solvent ligand in the protein.[13,14,15] However, this investigation provides independent and much stronger structural evidence, based on a very accurate crystal structure and a direct comparison of the crystallographic raw data and the ideal structure estimated by state-of-the-art QM calculations.

On the other hand, our calculations indicate that the corresponding oxidised structure is a mixture of $Mn^{2+}$and Mn^{3+}. The reason for this is that the Mn^{III} structure is reduced by electrons released by the intense X-rays during data collection. It is a well-known and serious problem that metal sites in crystal structures often are reduced during data collection.[46] In fact, this has been suggested several times for MnSOD.[14,47,48,56] This shows that the detailed structural data for the oxidised state are not reliable. Instead, the most accurate estimates of the dimensions of the oxidised active site in MnSOD actually is the QM estimates in Table 2, which should be accurate to within ~0.06 Å. Considering that the QM pK_a estimates[13,14,15] predicted the correct protonation state for the reduced structure, it is most likely that the oxidised has a metal-bound OH^- ion.

Moreover, our calculations show that it is no structural problem that the metal-bound solvent molecule accepts a hydrogen bond from $N^{\varepsilon 2}$ of Gln-146 when the solvent ligand is water. Already in the vacuum structure, the water ligand tilts so that it forms an angle of 68° to the Mn–O_{Sol} bond. In the crystal, this angle increases by 4°, giving a normal hydrogen bond between O_{Sol} and Gln-146, and a distance of 2.2 Å between the two hydrogen atoms. In fact, the distortion of the extra atom in water is very small in energy terms, less than 1 kJ/mole, which means that the enzyme does not destabilise the reduced state of MnSOD (decrease the reduction potential) by more than 10 mV, owing to this interaction.

Our MD simulations confirm this type of structure is stable also in long simulations and therefore probably can be trusted. Moreover, they show that the two hydrogen atoms on the water ligand alternates frequently in forming the hydrogen bond to the non-coordinating $O^{\delta 1}$ atom of the

Asp-167 ligand.

Finally, we have examined if the extra hydrogen atom on the water ligand may affect the binding of the superoxide substrate. Our MD simulations indicate that this is not the case: We obtain a very similar binding of superoxide to both the oxidised (with a OH^- ligand) and reduced form (with a water ligand) of the enzyme. On the other hand, we obtain two different binding modes of $O_2^{-\bullet}$ in our simulations. In most simulations, $O_2^{-\bullet}$ prefers to bind directly to the Mn ion (~2.2 Å distance), forming hydrogen bonds to Tyr-34 and to the water ligand in the reduced state. However, in two simulations, $O_2^{-\bullet}$ instead binds in the second coordination sphere, ~5 Å from Mn. This conformation is also stabilised by hydrogen bonds to Tyr-34, but not to the water ligand. This binding site is close to a second-sphere site suggested by NMR studies of FeSOD (~7.5 Å from Fe).[2,56] However, this binding mode reorganises during longer simulations, indicating that the first-sphere coordination probably is more favourable.

The stability of the second-sphere binding mode may be related to the conformation of the conserved His-30 residue. The most favourable binding seems to be obtained when the $N^{\delta 1}$ atom of this residue is pointing towards Tyr-34, which is observed in the second (but not the first) subunit of reduced MnSOD. This indicates that there may be a switch in the enzyme that may enhance or inhibit the second-sphere binding of substrates by changing the conformation of His-30.

Finally, it should be pointed out that the detailed structures of the binding modes of $O_2^{-\bullet}$ to MnSOD are quite preliminary at present (especially the first-sphere binding, which involves Mn–$O_2^{-\bullet}$ interactions that are very hard to model by classical methods). We currently develop and calibrate methods that will allow us to give a more accurate description of this interaction in the protein and to estimate the relative affinity of the two binding modes in the different oxidation states of the enzyme.

Acknowledgements

This investigation has been supported by the Swedish research council, by computer resources of Lunarc at Lund University, and by the project LC512 of MSMT CR (LR). We thank Prof. G. B. Jameson, Massey, for generously providing us the crystallographic structure factors for the two crystal structures of MnSOD.

References

(1) Miller, A.-F.; Sorkin, D. L. *Comments Mol. Cell Biophys.* **1997**, *9*, 1-48.

(2) Miller, A.-F. In *Handbook of Metalloproteins*; Messerschmidt, A; Huber, R.; Wieghardt, K.; Poulos, T.; Eds.; John Wiley & Sons: Chichester, 2001, pp 668-692.

(3) Stroupe, M. E.; DiDonato, M.; Tainer, J. A. In *Handbook of Metalloproteins*; Messerschmidt, A; Huber, R.; Wieghardt, K.; Poulos, T.; Eds.; John Wiley & Sons: Chichester, 2001, pp 941-951.

(4) Bordo, D.; Pesce, A.; Bolognesi, M.; Stroppolo, M. E.; Falconi, M.; Desideri, A. In *Handbook of Metalloproteins*; Messerschmidt, A; Huber, R.; Wieghardt, K.; Poulos, T.; Eds.; John Wiley & Sons: Chichester, 2001, pp 1284-1300.

(5) Wuerges, J.; Lee, J.-W.; Yim, Y.-I.; Yim, H.-S.; Kang, S.-O.; Carugo, K. D. *Proc. Natl. Acad. Sci. U. S. A.* **2004**, *101*, 8569-8574.

(6) Getzoff, E. D.; Tainer, J. A; Stempien, M. M.; Bell, G. I.; Hallewell, R. A. *Proteins* **1989**, *5*, 322-336.

(7) Steinman, H. M.; Weinstein, L.; Brenowitz, M. *J. Biol. Chem.* **1994**, *269*, 28629-28634.

(8) Chance, B.; Sies, H.; Boveris, A. *Physiol. Rev.* **1979**, *59*, 527-605.

(9) Bull, C.; Fee, J. A. *J. Am. Chem. Soc.* **1985**, *107*, 3295-3304.

(10) Miller, A.-F.; Padmakumar, K.; Sorkin, D. L.; Karapetian, A.; Vance, C. K. *J. Inorg. Biochem.* **2003**, *93*, 71-83.

(11) Stallings, W. C; Metzger, A. L.; Pattridge, K. A.; Fee, J. A.; Ludwig, M. L. *Free Radic. Res.* **1991**, *12-13*, 259-268.

(12) Whittaker, M. M.; Ekberg, C. A.; Edwards, R. A.; Baker, E. N.; Jameson, G. B; Whittaker, J. W. *J. Phys. Chem. B* **1998**, *102*, 4668-4677.

(13) Fisher, C. L.; Chen, J.-L.; Li, J.; Bashford, D.; Noodleman, L. *J. Phys. Chem.* **1996**, *100*, 13498-13505.

(14) Li, J.; Fisher, C. L.; Konecny, R.; Bashford, D.; Noodleman, L. *Inorg. Chem.* **1999**, *38*, 929-939.

(15) Han, W.-G.; Lovell, T.; Noodleman, L. *Inorg. Chem.* **2002**, *41*, 205-218.

(16) Anderson, B. F.; Edwards, R. A; Whittaker, M. M.; Whittaker J. W.; Baker, E. N.; Jameson G. B. To be published, PDB files 1ix9 and 1ixb.

(17) Ryde, U.; Olsen, L.; Nilsson, K. *J. Comput. Chem.* **2002**, *23*, 1058-1070.

(18) Ryde, U.; Nilsson, K. *J. Mol. Struct.* **2003**, *632*, 259-275.

(19) Kleywegt, G. J.; Jones, T. A. *Acta Crystallogr. D* **1998**, *54*, 1119-1131.

(20) Pannu, N. S.; Read, R. J. *Acta Crystallogr. A* **1996**, *52*, 659-668.

(21) Adams, P. D.; Pannu, N. S.; Read, R. J.; Brunger, A. T. *Proc. Natl. Acad. Sci. U. S. A.* **1997**, *94*, 5018-5023.

(22) Brünger, A. T. *Methods Enzymol.* **1997**, *243*, 269-277.

(23) Alrichs, R.; Bär, M.; Häser, M.; Horn, H.; Kölmel, C. *Chem. Phys. Lett.* **1989**, *162*, 165.

(24) Brünger, A. T.; Adams, P. D.; Clore, G. M.; Delano, W. L.; Gros, P.; Grosse-Kunstleve, R. W.; Jiang, J.-S.; Kuszewski, J. I.; Nilges, M.; Pannu, N. S.; Read, R. J.; Rice, L. M.; Simonson; T.; Warren, G. L. Crystallography & NMR System, CNS, Version 1.0, Yale University, 2000.

(25) Ryde, U.; Nilsson, K. *J. Am. Chem. Soc.* **2003**, *125*, 14232-14233.

(26) Nilsson, K.; Ryde, U. *J. Inorg. Biochem.* **2004**, *98*, 1539-1546.

(27) Edwards, R. A.; Whittake, M. M.; Whittaker, J. W.; Baker, E. N.; Jameson, G. B. *Biochemistry* **2001**, *40*, 5622-4632.

(28) Jones, T. A.; Zou, J.-Y.; Cowand, W. E.; Kjeldgaard, M. *Acta Crystallogr. A* **1991**, *47*, 110-119.

(29) Becke, A. D. *Phys. Rev. A* **1988**, *38*, 3098-3100.

(30) Perdew, J. P. *Phys. Rev. B* **1986**, *33*, 8822-8824.

(31) Hehre, W. J.; Radom, L.; Schleyer, P. v. R.; Pople, J. A. *Ab initio molecular orbital theory*; Wiley-Interscience: New York, 1986.

(32) Schäfer, A.; Huber, C.; Ahlrichs, R. *J. Chem. Phys.* **1994**, *100*, 5829-5835.

(33) Sigfridsson, E.; Olsson, M.H.M.; Ryde, U. *J. Phys. Chem. B* **2001**, *105*, 5546-5552.

(34) Olsson, M.H.M.; Ryde, U. *J. Am. Chem. Soc.* **2001**, *123*, 7866-7876.

(35) Shen, Y.; Ryde, U. *J. Inorg. Biochem.* **2004**, *98*, 878-895.

(36) Söderhjelm, P.; Volbeda, A.; Fontecilla-Camps, J. C.; Ryde, U. *J. Mol. Struct.*, submitted.

(37) Ryde, U.; Olsson, M. H. M.; Roos, B. O.; Borin-Carlos, A. *Theor. Chem. Acc.*, **2001**,*105*, 452-462.

(38) Reuter, Nat.; Dejaegere, A.; Maigret, B.; Karplus, M. *J. Phys. Chem.* **2000**, *104*, 1720-1735.

(39) Ryde, U. *J. Comput.-Aided Mol. Design* **1996**, *10*, 153-164.

(40) Case, D. A.; Darden, T. A.; Cheatham, T. E; Simmerling, C. L.; Wang, J.; Duke, R. E.; Luo,

R.; Merz, K. M.; Wang, B.; Pearlman, D. A.; Crowley, M.; Brozell, S.; Tsui, V.; Gohlke, H.; Mongan, J.; Hornak, V.; Cui, G.; Beroza, P.; Schafmeister, C.; Caldwell, J. W.; Ross, W. S.; Kolman, P. A. AMBER 8, University of California, San Francisco, 2004.

(41) Duan, Y.; Wu, C., Chowdhury, S.; Lee, M. C.; Xiong, G.; Zhang, W.; Yang, R.; Cieplak, P.; Luo, R.; Lee, T.; *J. Comput. Chem.* **2003**, *24*, 1999-2012.

(42) Berendsen, H. J. C.; Postma, J. P. M.; van Gunsteren, W. F.; DiNola, A.; Haak, J. R. *J. Chem. Phys.* **1984**, *81*, 3684-3690.

(43) Sigfridsson, E.; Ryde, U. *J. Comput. Chem.* **1998**, *19*, 377-395.

(44) Nilsson, K.; Lecerof, D.; Sigfridsson, E.; Ryde, U. *Acta Crystallogr. D* **2003**, *59*, 274-289.

(45) Seminario, J. M. *Int. J. Quantum Chem.* **1996**, *30*, 59-65.

(46) Wilmot, C. M.; Sjögren, T.; Carlsson, G. H.; Berglund, G. I.; Hajdu, J. *Methods Enzymol.* **2002**, *353*, 301-318.

(47) Whittaker, J. W.; Whittaker, M. M. *J. Am. Chem. Soc.* **2002**, *113*, 5528-5540.

(48) Jackson, T. A.; Xie, J; Yikilmaz, E; Miller, A.-F.; Brunold, T. C. *J. Am. Chem. Soc.* **2002**, *124*, 10833-10845

(49) Yikilmaz, E.; Xie, J.; Brunold, T. C.; Miller A.-F. *J. Am. Chem. Soc.* **2002**, *124*, 3482-3483.

(50) Lah, M. S; Dixon, M. M.; Pattridge, K. A.; Stallings, W. C.; Fee, J. A.; Ludwig M. L. *Biochemistry* **1995**, *34*, 1646-1660.

(51) Whittaker, M. M.; Whittaker J. W. *Biochemistry* **1996**, *35*, 6762-6770.

(52) Jackson, T. A.; Karapetian, A.; Miller, A.-F.; Brunold, T. C. *J. Am. Chem. Soc.* **2004**, *126*, 12477-12491.

(53) Rulíšek, L.; Jensen, K. P.; Lundgren, K.; Ryde, U. *J. Comput. Chem.*, in press.

(54) Borgstahl, G. E.; Pokross, M.; Chehab, R.; Sekher, A.; Snell, E. H. *J. Mol. Biol.* **2000**, *296*, 951-959.

(55) Edwards, R. A.; Whittaker, M. M.; Whittaker, J. W.; Jameson, G. B; Baker, E. N. *J. Am. Chem. Soc.* **1998**, *120*, 9684-9685.

(56) Vatyam, S.; Byrd, R. A.; Miller, A.-F. *Magn. Reson. Chem.* **2000**, *38*, 536-542.

(57) Miller, A.-F. *Curr. Opin. Chem. Biol.* **2005**, *8*, 162-168.

Table 1. Quality criteria of the quantum refinements. ΔE_{QM1} is the energy difference (in kJ/mole) between structures optimised in the protein and in vacuum, calculated with or without the model of Gln-146. $\Sigma\Delta r$ is the sum of the unsigned difference in the Mn–ligand distances (in Å) between the quantum refined structure and the optimised vacuum structure or the original crystal structure. Ligand *R* is the real-space *R* factor of the solvent ligand. The best values for each protein is highlighted in bold face.

Mn ox state	Ligand	R_{free}	R	Ligand R	ΔE_{QM1}	$\Sigma\Delta r$ vacuum	$\Sigma\Delta r$ Crystal
Reduced structure							
II	H_2O	**0.2155**	**0.2078**	**0.051**	**33.7**	**0.19**	**0.05**
II	OH^-	0.2157	0.2079	0.056	93.5	0.62	0.16
1ixb		0.2158	0.2077				
Oxidised structure							
III	AspH–OH^-	0.2128	0.2081	0.052	54.4	0.35	0.25
III	H_2O	0.2126	0.2081	0.048	98.7	0.37	0.15
III	OH^-	0.2130	0.2082	0.057	43.2	**0.18**	0.32
II	H_2O	**0.2122**	0.2080	0.041	**40.0**	0.24	**0.11**
II	OH^-	0.2125	**0.2079**	**0.041**	74.3	0.56	0.12
1ix9		0.2125	0.2079				

Table 2. The Mn–ligand distances (in Å) in the various structures (original crystal structures, quantum refined structures, and vacuum optimised structures). His1, His2, and His3 correspond to His-26, His-81, His-171 in the considered MnSOD structure from *E. coli*.

		Distance (in Å) from Mn to				
		N_{His1}	N_{His2}	N_{His3}	O_{Asp}	O_{Sol}
Reduced structure						
II	H_2O	2.18	2.13	2.16	2.04	2.27
II	OH^-	2.19	2.14	2.16	2.06	2.15
1ixb	subunit 1	2.17	2.13	2.14	2.05	2.27
	subunit 2	2.18	2.15	2.13	2.04	2.26
Oxidised structure						
II	H_2O	2.16	2.14	2.12	2.03	2.18
II	OH^-	2.17	2.15	2.13	2.05	2.05
III	AspH–OH^-	2.12	2.12	2.10	2.03	1.96
III	H_2O[a]	2.11	2.12	2.11	1.98	2.08
III	OH^-	2.13	2.13	2.11	1.99	1.87
1ix9	subunit 1	2.15	2.14	2.12	2.02	2.12
	subunit 2	2.14	2.14	2.12	2.03	2.16
Vacuum without Gln						
II	H_2O	2.23	2.20	2.17	2.05	2.23
II	OH^-	2.34	2.28	2.28	2.08	1.98
III	AspH–OH^-	2.02	2.06	2.06	2.07	1.85
III	H_2O[a]	2.02	2.01	2.15	1.89	1.99
III	OH^-	2.09	2.13	2.13	1.96	1.78

[a] The $H–O_{Sol}$ distance has been constrained in this calculations to 1.07 Å.

Table 3. Hydrogen-bond distances in the molecular dynamics simulations of reduced and oxidised MnSOD. We have followed the distances between the two (one in OH^-) hydrogen atoms in the solvent ligand and the Asp-167 $O^{\delta 1}$ atom, and between the $H^{\varepsilon 21}$ atom in Gln-146 and the oxygen atom of the solvent ligand during a 1 ns MD simulation. We report the minimum, maximum, and average distances, as well as the standard deviation. As a comparison, it can be mentioned that the corresponding values for the $Mn–O_{Sol}$ distance are 1.87, 2.36, 2.08, and 0.09 Å.

Distance (Å)	$H_{Sol1}–O_{Asp}$		$H_{Sol2}–O_{Asp}$		$H_{Gln}–O_{Sol}$	
Subunit	1	2	1	2	1	2
$Mn^{II}–H_2O$						
Average	2.49	2.44	2.52	2.38	2.15	2.09
Minimum	1.80	1.75	1.86	1.76	1.82	1.72
Maximum	3.22	3.33	3.68	3.39	2.48	2.46
Standard deviation	0.36	0.34	0.38	0.37	0.17	0.17
$Mn^{III}–OH$						
Average	2.06	2.03			2.09	2.08
Minimum	1.68	1.75			1.83	1.82
Maximum	3.14	2.77			2.70	2.40
Standard deviation	0.22	0.22			0.18	0.13

Figure 1. The quantum system used in the calculations (illustrated by the $Mn^{3+}Im_3AcOH$+Am model).

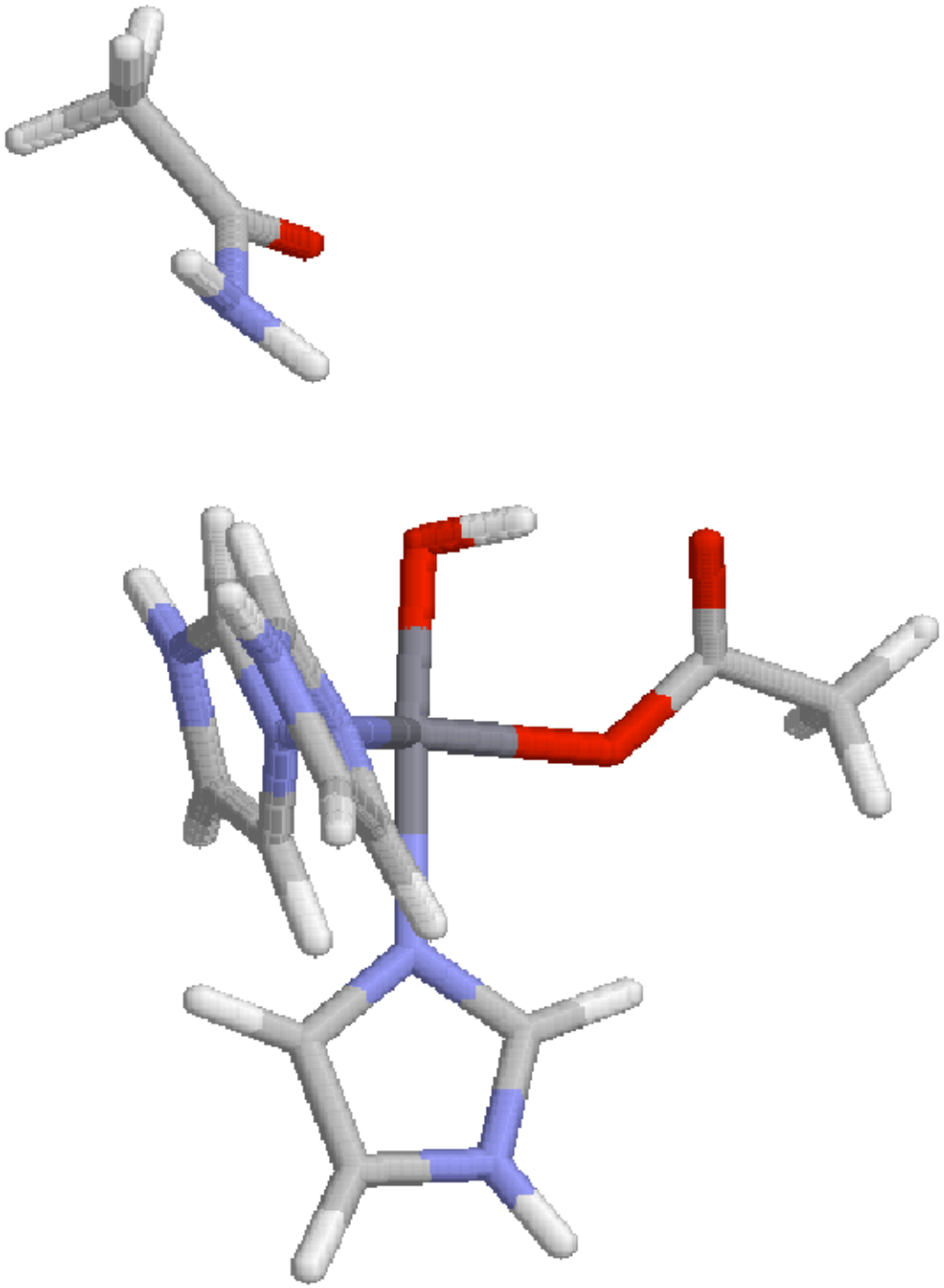

Figure 2. A comparison of the quantum refined OH^- (green) and water (red/yellow/magenta) structures in the reduced protein (the two structures superimpose to a large extent). The Mn ion is marked by a green or yellow cross near the centre of the figure. The oxygen atom of the ligand is a green or red cross in the top of the figure. His-26 (bottom), His-171 (left), His-81 (almost from the side of the imidazole ring), and Asp-167 (right) are also included. The figure also shows the $f_o - f_c$ difference maps of the two structures at the 3.5 σ level: blue (positive) and red (negative) for the water structure and green (positive) and yellow (negative) for OH^- structure.

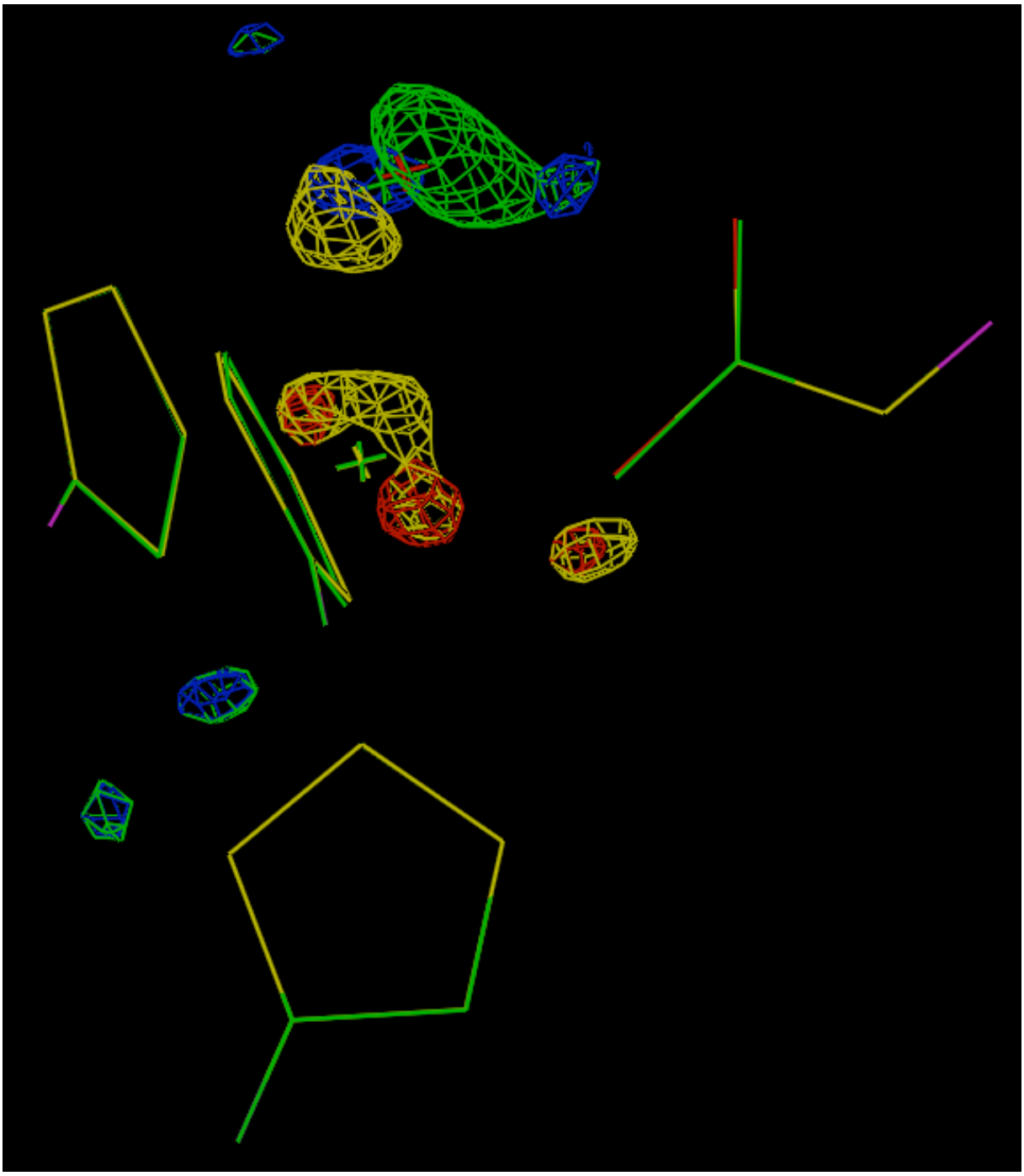

Figure 3. Residues and hydrogen bonds around the active site in the crystal structure of MnSOD.[16] Mn ligands are shown in thick coloured lines, other ligands in thinner lines, and water molecules as red balls. Coordinative bonds are shown in thick black lines, hydrogen bonds in thin, dotted lines.

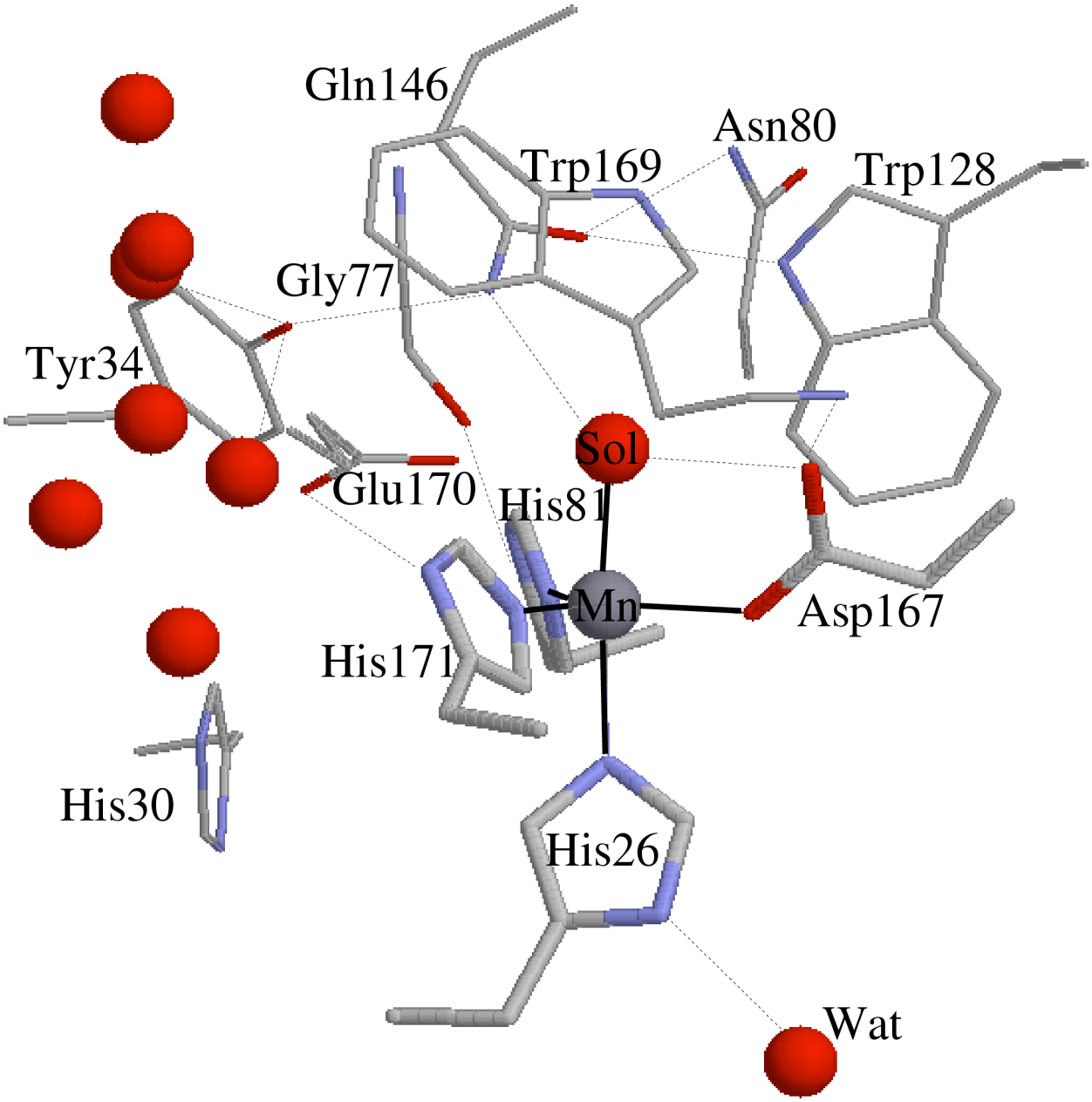

Figure 4. The structure of the quantum system in the quantum refined structures of (a) the oxidised structure with Mn^{3+}–OH^{-} (b) and the reduced structure with Mn^{2+}–H_2O.

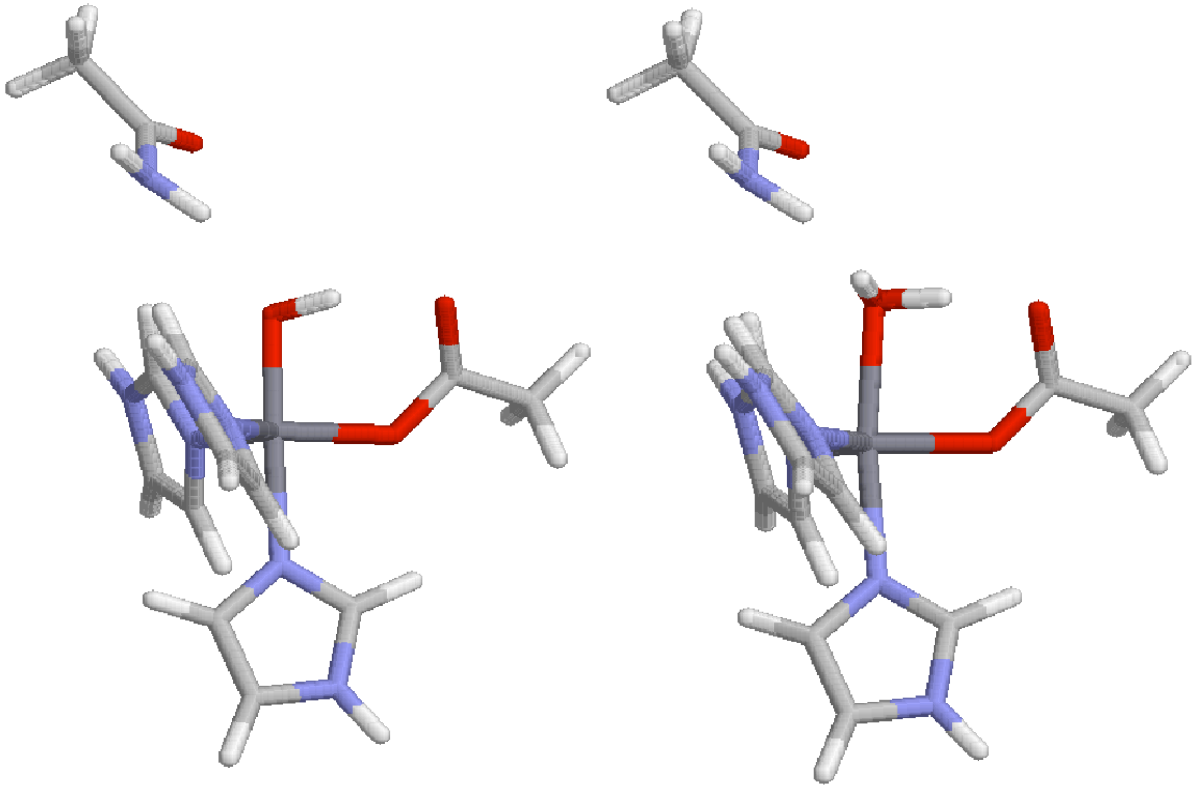

a b

Figure 5. The two binding modes of $O_2^{-\bullet}$ to MnSOD observed in the molecular dynamics simulations. The metal ion and the $O_2^{-\bullet}$ molecule are shown as balls, the Mn ligands, as thick stick, whereas His-30, Tyr-34, Gln-147, as well as a few nearby water molecules are shown as thin sticks.

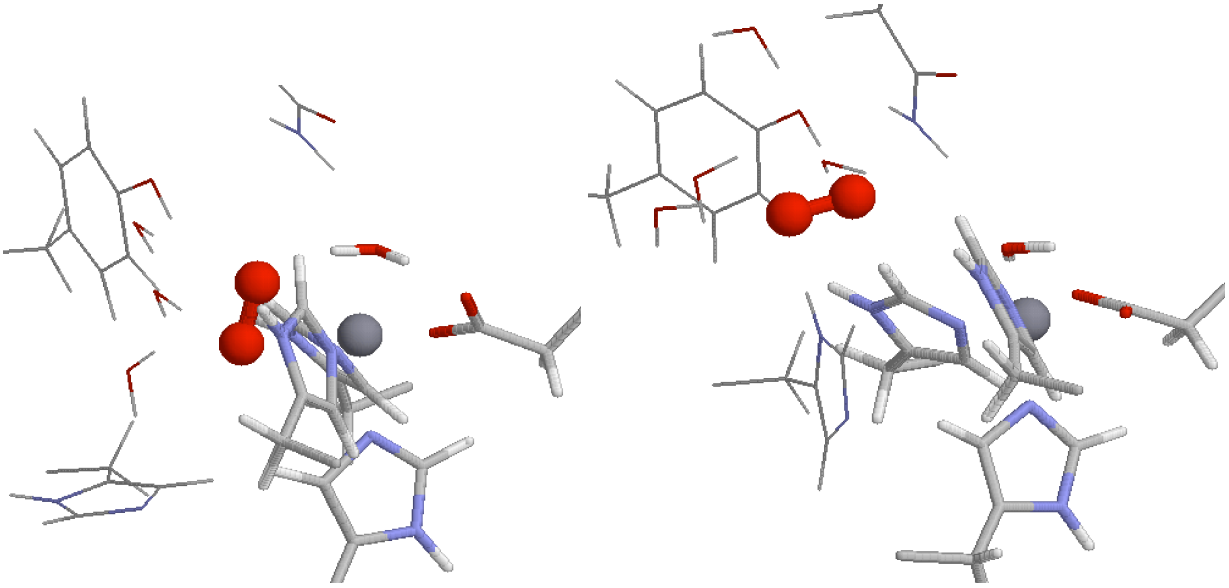

a b